Pergamon

PII: S0038-092X(96)00157-0

Solar Energy Vol. 60, No. 5, pp. 291–300, 1997

0038-092X/97 $17.00 + 0.00

DEVELOPMENT OF A FLOW DISTRIBUTION AND DESIGN MODEL FOR TRANSPIRED SOLAR COLLECTORS

C. DYMOND * and C. KUTSCHER **,†
* American Samoa Territorial Energy Office, Pago Pago, AS 96799, U.S.A. and
** National Renewable Energy Laboratory, 1617 Cole Boulevard, Golden, CO 80401, U.S.A.
(kutscher@tcplink.nrel.gov)

(Received 15 January 1996; revised version accepted 28 August 1996)
(Communicated by DOUG HITTLE)

Abstract—Unglazed, transpired solar collectors offer a low-cost, high-efficiency means for preheating outside air for ventilation and crop drying applications. Although large building wall applications for these collectors have generally performed well in the field, many have exhibited poor flow distribution which can prevent maximum efficiency from being achieved. The objective of this work was to develop a computer model which would run quickly on a personal computer and allow designers of transpired collectors to easily adjust geometric parameters to achieve reasonable flow uniformities and to determine efficiencies. This paper describes how this model was developed and includes results from model runs. In order to allow the model to run quickly on the PC, pipe network methods were used to develop a set of simultaneous equations in the unknown flow rates. Previous research results on heat exchange effectiveness, pressure drop, and wind heat loss were incorporated. © 1997 Elsevier Science Ltd.

1. INTRODUCTION

Unglazed, transpired solar collectors offer a low-cost, high-efficiency means for preheating outside air for ventilation and crop drying applications. The overall heat transfer theory for this type of collector is described by Kutscher *et al.* (1993), and the results of heat exchange effectiveness and pressure drop measurements are provided in Kutscher (1992) and Kutscher (1994). A remaining issue was the poor flow distribution that has occurred in large building applications as shown by infrared photographs (Enermodal Engineering Limited, 1994). Such poor distribution can cause penalties in performance due to greater radiative and convective heat losses at hotter, flow-starved surfaces. This article describes the development of a computer program developed to allow designers to predict flow uniformity and efficiency.

The suitability of a computational fluid dynamics (CFD) model that directly solves the Navier–Stokes and energy equations was evaluated. However, because there are many entrance flows into the absorber wall that are related to the unknown surface temperatures in a non-linear way (the surface temperature is a result of a local radiation and convection balance and affects the flow distribution due to the buoyancy term), a CFD model would require very long run times. In fact, a model using the commercial TASCflow CFD code has recently been developed for research purposes at the University of Waterloo (Gunnewiek, 1994). To save on memory and computational time, that code assumes that there is a constant velocity header across the top of the wall such that, in the absence of wind, all flow in the plenum is vertically upward only. The model further assumes that the ratio of local radiative heat loss coefficient to local heat exchange effectiveness is everywhere constant. For a 2-D flow case (with nodes across the plenum depth and vertically upward, but with no flow in the sideways direction), the TASCflow model takes about an hour on a Sun IPX work station, reasonable for research purposes, but not for a design tool. A 3-D model would take much longer and would be prohibitive on a PC.

The goal here was to accurately model the variations in heat loss coefficient and heat exchange effectiveness across the absorber and have the capability to model not only a constant velocity header but the much more typical cases of a discrete outlet or a constant area header (both of which cause flow in the plenum to occur in both the sideways and vertical directions). A further key requirement was to have run times on a personal computer (66 MHz 486) of only a few minutes, so that the designer could easily make many parametric runs to investigate the effects of variations in hole size and spacing, wall height and width, plenum

†Author to whom all correspondence should be addressed.

depth, and weather conditions—variations which are not easily made in a CFD model. There is no need to solve the Navier–Stokes equations when the pressure drops across the absorber and in the plenum are known empirically. Because this is essentially a flow distribution problem, we decided to see if we could achieve our goals by applying the methods of pipe network modeling. Described by Acrivos *et al.* (1959), Bajura and Jones (1976), Pigford *et al.* (1983), Shen (1992), and others, these methods have typically been used for liquid flow pipe networks. Applying this technique to the case of distributed air flow across a porous surface and through a plenum is believed to be new. Additional details of this model can be found in Dymond (1994).

1.1. General description of the collector

The unglazed transpired collector (UTC) has a dark perforated surface through which air is drawn. Unlike typical solar air heaters, the UTC does not have a layer of glazing covering its front, and, unlike matrix collectors, it uses a single thin perforated sheet instead of a thick matrix for the solar absorber. The collector is typically mounted on the south side of the exterior of a building.

Figure 1 shows insolation heating the absorber surface through which air is heated as it is swept across the surface to the holes. The warmed air then moves up the plenum and is delivered to the building interior by a fan. A fan is necessary to overcome the pressure drop across the collector to drive the air through the absorber.

The absorber surface is most commonly a thin perforated aluminum sheet, although other materials have been used such as fabric (Schulz, 1988). The porosity of the collector surface is typically 0.5 to 2%.

The space behind the absorber (plenum) is a sealed box with only the south side made of the perforated material. The depth of the plenum varies from one collector design to another. Typical depths are between 5 and 30 cm. The back wall of the plenum is commonly the building's exterior surface.

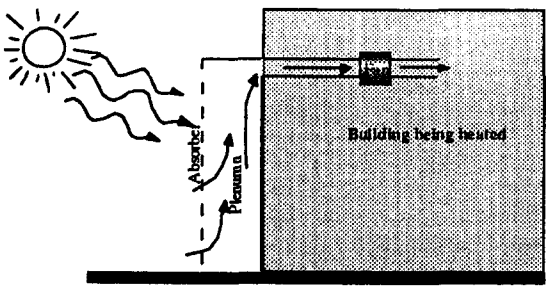

Fig. 1. Cross-section of an unglazed transpired collector and building.

2. MODEL DESCRIPTION

Determining the surface (absorber) temperature profile of the unglazed transpired collector requires that the flow through the collector be known. Flow rates through the absorber are then used in an energy balance of the absorber to determine the surface temperatures and the temperature of the air inside the collector plenum.

The model includes all four pressure drops in the system: friction across the collector, friction in the plenum, buoyancy in the plenum and acceleration of the fluid in the plenum (caused by the addition of air and convergence of the flow as it approaches the exit). The energy balance on the collector surface includes the significant energy transfers involved: solar radiation from the sun, infrared radiation between the collector surface and ground, infrared radiation between the collector surface and sky, wind-driven convective heat losses, and the energy delivered to the air stream. The effect of local variations in ambient pressure due to wind are not modeled, since experimental work has shown that this is a small effect in a well designed wall as long as the pressure drop across the absorber is at least 25 Pa.

2.1. Modeling algorithm

The algorithm used to model flow distribution for the unglazed transpired collector requires that the flow and temperature be solved iteratively, with one iterative cycle inside the other. First the flow distribution through the collector is determined iteratively using the linear theory method for pipe network modeling (Jeppson, 1976). Then the temperature distribution of the air flow through the collector is determined. The new temperatures are then used to re-evaluate the buoyancy term and air properties, and the flow distribution calculation is started again. Convergence is reached when the temperature difference between successive iterations is less than some defined limit. Figure 2 is a flow chart of the process used.

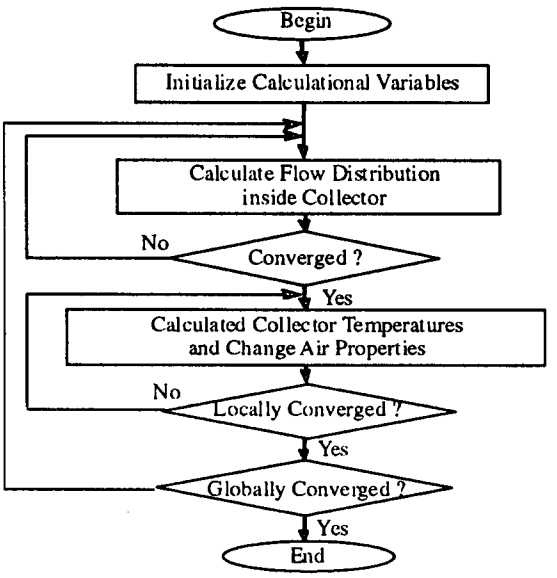

Fig. 2. General flow chart of the model.

2.2. *Applying the pipe network modeling algorithm*

Applying a pipe network to the unglazed transpired collector requires that the open plenum inside the collector be modeled as if it were a set of fictitious "pipes" arranged as shown in Fig. 3. The figure shows the interconnection of fictitious x-directional and y-directional pipes inside the plenum. The flow directions are assumed to be up and to the right in each pipe. At each junction of the pipes inside the plenum a z-directional pipe was assumed to be transferring air across the collector absorber. The concept of "pipes" is used here for conceptual visualization only to allow an easy analogy to pipe network problems in which continuity is required at pipe junctions and pressure drops are summed about pipe loops. The pressure drop for flow down a "pipe" in this case is based on the empirical result for flow between parallel plates.

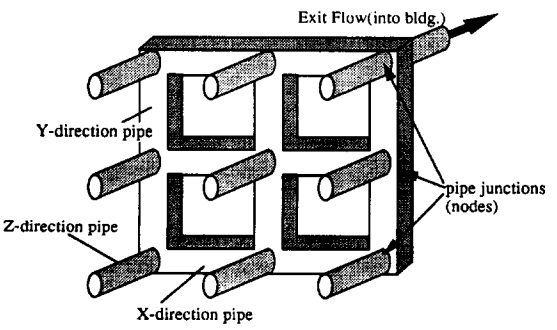

Fig. 3. An example of a 3 by 3 set of pipe junctions connected to form a pipe network.

The pipe network has M horizontal nodes (pipe junctions) and N vertical nodes. There are $(M-1)(N)$ horizontal x-directional pipes, $(M)(N-1)$ vertical y-directional pipes, and $(M)(N)$ z-directional pipes transporting air across the absorber. The network can have one exit along the top edge of the collector. (A constant area or constant velocity header across the top can also be modelled.) From this exit, air is drawn into the building interior. Only one discrete exit (or a single header) is possible for computational reasons that are explained later. The example used throughout is a model that is a 3 by 3 set of nodes with an exit in the top right corner as shown in Fig. 3. The N by M pipe nodes results in a network of $\{MN+(M-1)N+M(N-1)\}$ pipes for which the flow rates are unknown. The continuity equation is applied at each junction to give $M \times N$ linear equations. The conservation of mechanical energy is applied around x-directional loops and y-directional loops to give $\{(M-1)N+M(N-1)\}$ equations. Each loop begins outside the collector, passes through a z-directional pipe, then moves either along an x- or y-directional pipe to an adjacent junction where it travels through a z-directional pipe back out through the collector. The hydrostatic pressure difference between the two entry points is included in a buoyancy term which closes the loop equation.

2.3. *Conservation of mass (continuity) equations*

The continuity equation is used to generate a set of $M \times N$ equations for a matrix of pipes with M horizontal nodes and N vertical nodes. The equation which was used in the model is expressed in terms of volumetric flow of the air into and out of a pipe junction as follows:

$$\sum_{i=1}^{\text{No of flows}} \rho_i Q_i = 0. \tag{1}$$

In the example of a 3 by 3 pipe network, there are 21 pipes in which the flow is unknown. Applying the continuity equation provides nine of the 21 equations needed to define the flow.

2.4. *Conservation of mechanical energy (loop pressure drop) equations*

The conservation of mechanical energy in the form of Bernoulli's equation can be applied to a pipe network of steady-state incompressible flow by setting the sum of all pressure drops

(change in fluid energy) around any closed loop equal to zero. In our network of fictitious pipes, this is done by summing the pressure drops for loops which start outside the collector, travel through a z-directional pipe into the plenum, move either horizontally along an x-directional or vertically along a y-directional pipe to an adjacent node, and exit through the next z-directional pipe. For the loop shown in Fig. 4, this yields

$$\Delta P_8 + \Delta P_2 - \Delta P_9 = 0. \tag{2}$$

The negative sign in front of the ΔP_9 indicates that the loop path is in the opposite direction of the flow in pipe 9. Both ΔP_8 and ΔP_9 are comprised of only the pressure drop across the collector surface

$$\Delta P_8 = \Delta P_{\text{absorber}_8} \quad \Delta P_9 = \Delta P_{\text{absorber}_9}. \tag{3}$$

However, ΔP_2 is composed of the frictional pressure drop, net buoyancy pressure, and the change in the velocity pressure (acceleration pressure drop) in the plenum between nodes A and B. Thus ΔP_2 is given by

$$\Delta P_2 = \Delta P_{\text{friction}_2} + \Delta P_{\text{buoyancy}_2} + \Delta P_{\text{acceleration}_2}. \tag{4}$$

The entire conservation equation becomes

$$0 = \Delta P_{\text{absorber}_8} + \Delta P_{\text{friction}_2} + \Delta P_{\text{buoyancy}_2} + \Delta P_{\text{acceleration}_2} - \Delta P_{\text{absorber}_9}. \tag{5}$$

In order to solve for the flow rates in each of the pipes using matrix algebra, the equations must be linear. The expressions for the buoyancy pressure, and the frictional pressure drop for laminar flow inside the plenum are linear. However, the expressions for the pressure drop across the collector, turbulent frictional pressure drop in the plenum, and acceleration pressure drop are non-linear. How the non-linear pressure drop terms are linearized is described below. In the example 3 by 3 pipe network, applying the conservation of energy results in six x-directional pipe loop equations and six y-directional pipe loop equations. Including the nine equations developed using the conservation of mass, there are 21 unique equations which describe the 21 unknown flow rates.

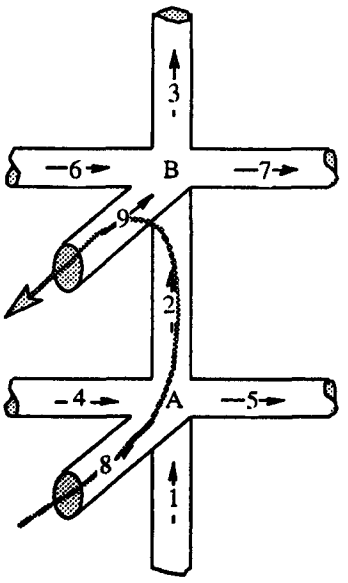

Fig. 4. Example of a loop.

2.4.1. Pressure drop through collector. The frictional pressure drop across the collector is based on the empirical correlation developed by Kutscher (1994). The pressure drop inside the z-directional pipes is given below in terms of volumetric flow rates.

$$\Delta P_{\text{absorber}} = 0.5\rho \frac{Q_{\text{face}}^2}{A_{\text{face}}^2}\left[6.82\left(\frac{1-\delta}{\delta}\right)Re_{\text{d}}^{-0.236}\right] \tag{6}$$

where Re_{d} is the Reynolds number of the air passing through the absorber and is calculated by

$$Re_{\text{d}} = \frac{Q_{\text{face}} d_{\text{hole}}}{A_{\text{face}} \delta \nu}. \tag{7}$$

Equation (6) is linearized by defining the following coefficient:

$$K'_{\text{absorber}} = 0.5\rho \frac{Q_{\text{face}}}{A_{\text{face}}^2}\left[6.82\left(\frac{1-\delta}{\delta}\right)Re_{\text{d}}^{-0.236}\right]. \tag{8}$$

Thus the linear equation describing the pressure drop across the collector absorber is given by

$$\Delta P_{\text{absorber}} = K'_{\text{absorber}} Q_{\text{face}} = K'_{\text{absorber}} Q_{\text{zpipe}}. \tag{9}$$

2.4.2. Friction inside collector plenum. The frictional pressure drop of air moving inside the plenum is handled by the same methods used to determine the flow rate in ducts (ASHRAE, 1993). The frictional pressure drop is

$$\Delta P = f \frac{L}{D_{\text{h}}} \frac{\rho Q^2}{2A^2} \tag{10}$$

where, for turbulent flow, f is approximated using a curve fit to the Moody diagram

$$f = aQ^{-b}. \tag{11}$$

For laminar flow the pressure drop is given by

$$f = \frac{64}{Re}. \tag{12}$$

The linearization coefficient for turbulent flow is defined by

$$K'_{\text{friction}} = f \frac{L}{D_h} \frac{\rho Q}{2A^2}. \tag{13}$$

Thus the linear equation describing the pressure drop across the collector is given by

$$\Delta P_{\text{friction}} = K'_{\text{friction}} Q_{\text{pipe}}. \tag{14}$$

Because the equation for the pressure drop of laminar flow is already linear, no linearization coefficient is necessary.

2.4.3. Buoyancy pressure drop. The model developed in this study is unique in its ability to handle non-uniform flow with buoyancy dependent on local variation in the temperature of the air inside the plenum. This term is not dependent on the flow rate inside the pipe; rather it is dependent on the change in the density of the air column inside the collector plenum. Because the air inside the plenum is warmer and lighter than the air outside the collector, the buoyancy force is positive in the y-direction. This force is only present in y-directional pipes since there is no vertical height difference from one end of an x-directional pipe to the other end. Thus for x-directional pipes, the buoyancy force is given by

$$\Delta P_{\text{buoyancy}} = 0 \tag{15}$$

and for y-directional pipes the buoyancy force is given by

$$\Delta P_{\text{buoyancy}} = (\rho_{\text{ambient}} - \rho_{\text{ypipe}}) g (h_{\text{ypipe}}) = \Delta \rho g h_{\text{ypipe}} \tag{16}$$

where h_{ypipe} is the length of the y-directional pipe.

2.4.4. Acceleration pressure drop. The fourth term in the conservation of mechanical energy loop equations is what we refer to as the acceleration pressure drop in the pipe between two nodes (junctions). This is the Bernoulli effect and is related to the change in kinetic energy. As the air in the plenum moves toward the building inlet (plenum outlet), the flow accelerates as a result of both mass addition and geometric convergence. This results in a significant drop in static pressure, and this term proved to be difficult to describe because the velocity of the air in the plenum is only known inside the pipes (not at the nodes). Because the fluid velocity is undefined at the nodes, the change in velocity pressure between one node and an adjacent node must be based on the changes in velocity pressures of nearby pipes. Initially, it was assumed that a simple offset would be adequate, and that the offset of the velocity pressure from the nodes to the pipes would not matter if the collector were modeled with a fine enough grid of fictitious pipes. However, this did not prove to be the case, and several assumptions about the fluid direction entering and exiting each node were needed.

To account for the acceleration of the fluid in the pipe accurately without artificially imposing a static pressure regain in pipes as the fluid turned and moved into another pipe, a method was developed which we refer to as the "streamline method" for estimating the acceleration pressure drop inside an open plenum modeled as a pipe network. This method follows the flow along a typical hypothetical streamline entering the first node of interest and leaving the second node. The primary assumption of this method is that the general direction the fluid travels is known. Secondary assumptions made in this method are that the density and acceleration between two nodes are constant.

Consider air moving in the pipe network as shown in Fig. 5. For the moment, we neglect the effects of the z-directional flows entering the pipe networks at the junctions A and B, thereby reducing the problem to just two-dimensional flow in the x-directional and y-directional pipes. To know the change in the velocity pressure between nodes A and B (the acceleration pressure drop in pipe 2) we need to know the velocity of the fluid at A and at B. Because we only know the flow rates in the pipes, we must therefore approximate the velocities at A and B.

Figure 5 shows a gray line which represents the hypothetical streamline of fluid moving through pipe 2. Prior to being in pipe 2, the

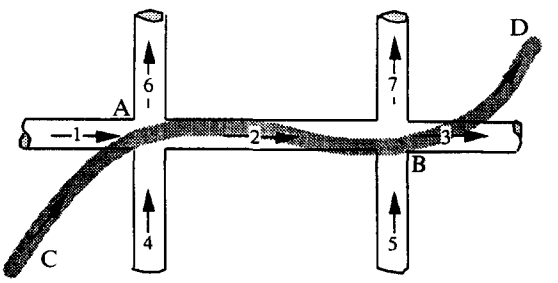

Fig. 5. The image of a streamline path superimposed on a pipe network.

flow came from either pipe 1, pipe 4, or both. After flowing through pipe 2, the fluid must exit node B through either pipe 3, pipe 7, or both. There is no knowledge of what fraction of the fluid in pipe 2 goes into pipe 7 or pipe 3, or what fractions of the flow in pipes 1 and 4 moved into pipe 2. Locations C and D are not physical locations in the pipe network; rather they represent the location where the fluid would be in an open plenum. Location C is used to describe the fluid before it enters node A, and location D is used to describe the fluid after it leaves node B.

The "streamline" method assumes that the velocity at node A can be approximated by the average velocity of the fluid at C and 2

$$V_A = \frac{(V_C + V_2)}{2} \tag{17}$$

and the velocity at node B is approximated by the average velocity of the fluid at 2 and D_3

$$V_B = \frac{(V_2 + V_D)}{2}. \tag{18}$$

To obtain the velocities at C and D, we apply conservation of momentum at each node. The acceleration pressure drop is then

$$\Delta P_{AB} = \tfrac{1}{2}\rho v_2 v_D - \tfrac{1}{2}\rho v_C v_2. \tag{19}$$

Details of this term are described in Dymond (1994).

2.5. *Flow distribution calculation*

Applying the continuity equation and the conservation of mechanical energy results in a set of equations which are linearly independent. For a pipe network of M by N inter-connected nodes there are $S = \{MN + (M-1)N + M(N-1)\}$ pipes with unknown flows. Applying the continuity equation results in MN equations, one for each pipe junction. Applying the conservation of energy results in $(M-1)N$ equations for the x-directional loops and $M(N-1)$ equations for the y-directional loops. The equations are written in matrix form as

$$\boldsymbol{K} \cdot \boldsymbol{Q} = \boldsymbol{C} \tag{20}$$

where $\boldsymbol{K}$ is the matrix containing all the coefficients, $\boldsymbol{Q}$ is the vector matrix containing all the unknown volumetric flow rates, and $\boldsymbol{C}$ is the solution vector containing all the constants

$$\boldsymbol{K} = \begin{bmatrix} K_{11} & K_{12} & K_{13} \\ K_{21} & K_{22} & K_{23} \\ K_{31} & K_{32} & K_{33} \end{bmatrix} \quad \boldsymbol{Q} = \begin{bmatrix} Q_1 \\ Q_2 \\ Q_3 \end{bmatrix} \quad \boldsymbol{C} = \begin{bmatrix} C_1 \\ C_2 \\ C_3 \end{bmatrix}. \tag{21}$$

The $\boldsymbol{K}$ matrix is set up as follows:

$$\mathrm{K} = \begin{bmatrix} \text{Continuity equations} \\ \vdots \\ \text{x-Loop conservation of energy equations} \\ \vdots \\ \text{y-Loop conservation of energy equations} \\ \vdots \end{bmatrix} \tag{22}$$

We solve for the S unknown flow rates by employing LU decomposition. Once the flow rates are known for each pipe in the network, the flow rates are used to re-calculate the K' terms (linearization terms), and the flow rates are solved for again.

This process continues until successive iterations result in the largest change in any flow rate from one iteration to the next being less than an accepted limit. In the program, this limit is defaulted to 0.1% of an average z-directional pipe velocity.

2.6. *Temperature calculation—the thermal energy balance*

All temperature calculations are made after the flow rates in each of the fictitious pipes have been determined. The following sections describe how an energy balance is used to calculate the absorber surface temperature and the temperature of the air entering the collector through the z-directional pipes, and how a marching solution is used to determine the temperature of the air in each of the x-directional and y-directional pipes inside the collector plenum.

2.6.1. Determining collector surface temperature. Once the flow rates through the collector have been determined, the temperatures of the absorber surface can be calculated by employing energy balances on the absorber. Figure 6 shows each of the energy quantities considered in the energy balance.

In order to solve for the absorber temperature, the infrared losses are taken from the Stefan–Boltzmann equation and linearized

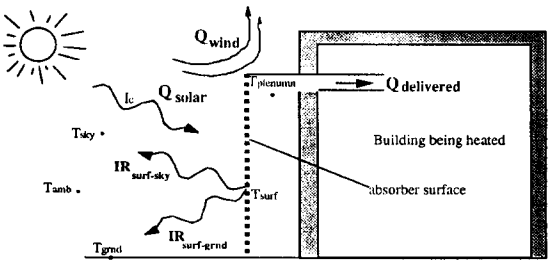

Fig. 6. Energy balance on absorber.

using the following expressions:

$$Q_{\text{surf-sky}} = U_{\text{ss}}(T_{\text{surf}} - T_{\text{sky}}) \tag{23}$$

$$Q_{\text{surf-grnd}} = U_{\text{sg}}(T_{\text{surf}} - T_{\text{grnd}}) \tag{24}$$

where

$$U_{\text{ss}} = F_{\text{ss}}\epsilon\sigma(T_{\text{surf}}^2 + T_{\text{sky}}^2)(T_{\text{surf}} + T_{\text{sky}}) \tag{25}$$

$$U_{\text{sg}} = F_{\text{sg}}\epsilon\sigma(T_{\text{surf}}^2 + T_{\text{grnd}}^2)(T_{\text{surf}} + T_{\text{grnd}}). \tag{26}$$

The convective heat loss is given by

$$Q_{\text{convective}} = U_{\text{w}}(T_{\text{surf}} - T_{\text{amb}}) \tag{27}$$

where

$$U_{\text{w}} = C_{\text{f}}[0.82(U_\infty/v_0^2)H\rho c_{\text{p}} v_0]. \tag{28}$$

This wind heat loss coefficient is an analytical result from laminar boundary layer theory for flow over a flat plate with suction (Kutscher *et al.*, 1993) and was verified experimentally by Kutscher (1992). C_{f} is the corrugation factor, an empirical coefficient that represents the ratio of wind heat loss for a corrugated absorber to that of a flat absorber and will be described in a future article. The ground temperature is entered as a user input, and the sky temperature is calculated using the dew point temperature correlation from ASHRAE (1993):

$$T_{\text{sky}} = T_{\text{ambient}}(0.689 + 0.0056T_{\text{dewpoint}} + 0.000073T_{\text{dewpoint}}^2 + 0.00012P_{\text{ambient}})^{0.25}. \tag{29}$$

Energy gained by the absorber is set equal to the energy lost:

$$Q_{\text{solar}} = Q_{\text{delivered}} + Q_{\text{surf-sky}} + Q_{\text{surf-grnd}} + Q_{\text{convection}} \tag{30}$$

or

$$\alpha I_{\text{c}} = \dot{m}c_{\text{p}}(T_{\text{plenum}} - T_{\text{amb}}) + U_{\text{ss}}(T_{\text{surf}} - T_{\text{sky}}) + U_{\text{sg}}(T_{\text{surf}} - T_{\text{grnd}}) + U_{\text{w}}(T_{\text{surf}} - T_{\text{amb}}) \tag{31}$$

where T_{plenum} is taken from the definition of absorber heat exchange effectiveness:

$$T_{\text{plenum}} = \epsilon_{\text{hx}}(T_{\text{surf}} - T_{\text{amb}}) + T_{\text{amb}}. \tag{32}$$

The heat exchange effectiveness is obtained from an empirical correlation developed by Kutscher (1994):

$$\epsilon_{\text{hx}} = 1 - \exp\left[\frac{\delta - 1}{G''C_{\text{p}}}\frac{k}{d}Nu_{\text{d}}\right] \tag{33}$$

where

$$Nu_{\text{d}} = 2.75\left[\left(\frac{p}{d}\right)^{-1.21} Re_{\text{d}}^{0.430} + 0.11\delta\, Re_{\text{d}}\left(\frac{U_\infty}{v_0}\right)^{0.480}\right]. \tag{34}$$

The temperature of the air entering the plenum, T_{plenum}, is solved for, and then T_{surf} is determined from

$$T_{\text{surf}} = \left(\frac{\alpha I_{\text{c}} + \dot{m}_{\text{p}}\epsilon_{\text{hx}}T_{\text{amb}} + U_{\text{sg}}T_{\text{grnd}} + U_{\text{w}}T_{\text{amb}}}{\dot{m}C_{\text{p}}\epsilon_{\text{hx}} + U_{\text{sg}} + U_{\text{w}}}\right). \tag{35}$$

This requires iteration since T_{surf} is contained in the heat loss coefficients. The result is that the surface temperatures and the temperatures of the air entering the plenum at each of the z-directional pipes of the M by N grid are known.

2.6.2. Determining plenum air temperature. The assumption is made that once the air is inside the plenum there is no radiative or conductive heat transfer to the air from the wall behind the plenum or the back side of the absorber. The building wall is assumed to be insulated, and therefore the heat transfer to the air stream is negligible. The absorber surface is somewhat hotter than the air inside the plenum and therefore some additional heat transfer from the absorber to the plenum flow is possible, although we expect this to be small because of the injection effect on the absorber side of the plenum and the laminarization induced by acceleration. (Recent interesting computational fluid dynamics simulations by Gunnewiek (1994) indicated that additional heat transfer to the bulk flow from the back side of the absorber surface can be significant near the top of a wall with buoyancy-driven non-uniform flow, i.e. with flow starvation near the top. However, no attempt was made to develop a back-surface heat transfer correlation. If data on back surface heat transfer should become

available, we hope to incorporate it into our model.)

The air inside the plenum is a combination of the air entering the collector through the z-directional pipes, each potentially at a different temperature. The temperatures in all of the x- and y-directional pipes between these z-directional pipes are calculated by assuming that the air temperature leaving a junction is the same as the perfectly mixed temperature of the air entering the junction. A marching solution is used to calculate the temperature in each pipe. The temperatures are calculated from the bottom left corner of the collector to the top right corner where the exit is located. Because we start at the lower left corner and move in the same direction as the fluid flows, at each step the temperature at the junction is based on the temperatures of flows that have been previously determined.

3. MODEL RESULTS

3.1. Example collector

The computer program generates three absorber profiles. The first profile is the flow distribution of the air entering the absorber surface, the second profile, is the temperature distribution of the collector surface, and the third profile is of the local collector efficiencies. Presented here are the three profiles for an example collector model. The example collector is 5 m high by 10 m wide with a single exit in the top center of the collector. Using symmetry, it is modeled as if it were 5 m high by 5 m wide with an exit in the top right corner of the collector.

Figure 7 is a plot of the face velocity data generated by running the model for the example collector. The x-axis of the plot shows the horizontal position of the collector (Width), the y-axis of the plot shows the vertical position of the collector (Height), and the z-axis shows the velocity of the air as it enters the absorber surface.

The most obvious feature in Fig. 7 is the large rise in face velocity near the top center of the collector. This large peak is immediately in front of the exit where the air flows directly into the interior of the building. At locations away from this top center of the collector the air must travel inside the collector plenum experiencing the three plenum pressure drops: acceleration, friction, and buoyancy. As a result, the pressure drop across the absorber, and therefore the face velocity, decrease dramatically the further away it is from the exit.

Along the left and right sides of the collector there is less flow through the top of the collector than through the bottom of the collector. This is because of the buoyancy effect. Figure 7 shows the local flow starvation in the top left and top right hand corners of the collector which is characteristic of a collector with a single top center exit. Because of the location of these points at the top of the wall, the buoyancy effect is greatest and yet they are also at a considerable distance from the inlets so that frictional and acceleration effects also tend to lower the flow rate here.

The temperature profile of the unglazed transpired collector (Fig. 8) is a mirror image of the face velocity profile. The larger the air flow through the collector, the better the heat is transferred away from the absorber which results in a lower temperature of the absorber.

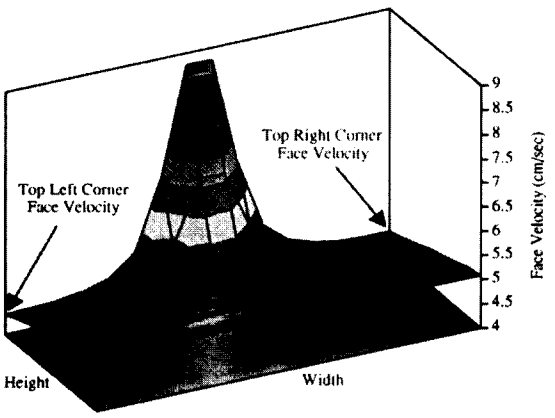

Fig. 7. Face velocity profile of example collector.

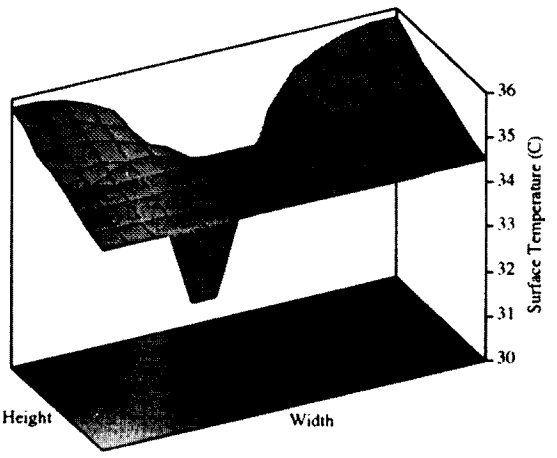

Fig. 8. Surface temperature profile of example collector.

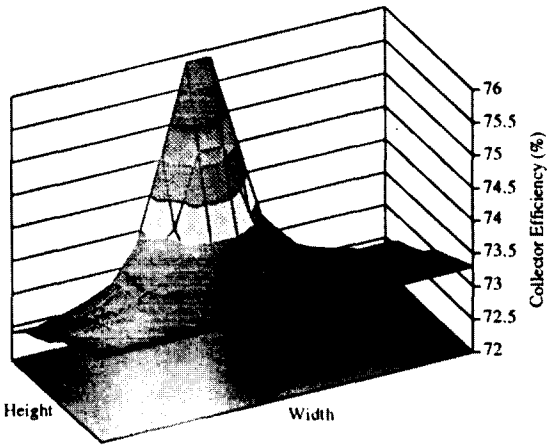

Fig. 9. Efficiency profile of example collector.

The top left and right corners of the collector are warmer than the rest of the collector because of flow starvation as described previously.

The efficiency profile of the unglazed transpired collector (Fig. 9) has the same shape and form as the face velocity profile. The larger the air flow through the collector, the better the heat is transferred away from the absorber which results in a higher collector efficiency.

4. SUMMARY AND CONCLUSIONS

The pipe network method used in this study proved capable of modeling the flow rates and temperatures of an unglazed transpired collector wall and led to a computer program with very reasonable run times. Typical pipe network methods used to model municipal water pipes only include the pressure drops due to friction, changes in elevation, and across pumps. Employing the pipe network model to the air flow through the unglazed transpired collector required inclusion of the additional pressure drops due to the acceleration of the air in the plenum, the buoyancy of the heated air, and pressure drop across the absorber.

The model required that the acceleration pressure drop between two pipes be handled using only flow rates in nearby pipes. The "streamline" method presented here utilizes conservation of momentum. It relies on a knowledge of where the fluid is going and, as a result, there can be only one plenum exit (discrete or header) placed along the top edge of the plenum. This limitation is fairly minor since most transpired collector designs have an exit along the top edge of the plenum.

The computer program, named TCFLOW, is now used by Conserval Engineering, Inc. in the design of all their new "Solarwall" installations Hollick (1995). This study has provided a model of the unglazed transpired solar collector that is useful both as a design tool and as a tool for research and development of better, more efficient collector designs.

NOMENCLATURE

a	coefficient for curve fit to Moody diagram ($m^3 s^{-1}$)
A	cross-sectional area of "pipe" (m^2)
A_{face}	area of section of collector (m^2)
b	coefficient for curve fit to Moody diagram ($m^3 s^{-1}$)
$\boldsymbol{C}$	vector of constant terms in matrix equation
C_f	corrugation factor; ratio of wind heat loss from corrugated absorber to that of a flat absorber
c_p	specific heat of air ($J kg^{-1} K^{-1}$)
D_h	hydraulic diameter of "pipe" (m^2)
d	diameter of holes in absorber surface (m^2)
f	friction factor
F_{sg}	view factor of collector surface to ground
F_{ss}	view factor of collector surface to sky
g	gravitational acceleration ($9.8 m s^{-2}$)
G''	suction mass flow rate based on A_{face} ($kg s^{-1} m^{-2}$)
H	height of collector (m)
h_{ypipe}	length (height) of y-directional "pipe" (m)
I_c	insolation on collector surface ($W m^{-2}$)
$\boldsymbol{K}$	coefficient matrix
$K'_{absorber}$	linearization coefficient for absorber pressure drop term
$K'_{friction}$	linearization coefficient for frictional pressure drop term
k	thermal conductivity of air ($W m^{-1} K^{-1}$)
L	length of "pipe" (m)
M	number of horizontal nodes
m	mass flow rate of air ($kg s^{-1}$)
Nu_d	Ud/k_{air} = Nusselt number
N	number of vertical nodes
P	pressure (Pa)
p	pitch, distance between holes in absorber (m)
Q	volumetric flow rate ($m^3 s^{-1}$)
$Q_{convective}$	convective heat loss of collector ($W m^{-2}$)
$Q_{delivered}$	energy delivered by collector ($W m^{-2}$)
Q_{face}	flow rate as it approaches the face of the collector ($m^3 s^{-1}$)
Q_{solar}	total energy absorbed by the absorber surface from solar radiation ($W m^{-2}$)
$Q_{surf-sky}$	radiant heat loss from absorber to sky ($W m^{-2}$)
$Q_{surf-grnd}$	radiant heat loss from absorber to ground ($W m^{-2}$)
Q_{zpipe}	flow rate through z-directional pipe ($m^3 s^{-1}$)
Re	Reynolds number
Re_d	Reynolds number for air flowing through the holes in the absorber
S	number of unknown flowrates
$T_{ambient}$	ambient air temperature (K)
$T_{dewpoint}$	dewpoint temperature (K)
T_{grnd}	ground temperature (K)
T_{plenum}	plenum air temperature (K)
T_{sky}	plenum air temperature (K)
T_{surf}	absorber surface temperature (K)
U	convective heat transfer coefficient for suction air based on log mean temperature difference and non-hole absorber area ($W m^{-2} K$)

U_∞ wind speed (m s^{-1})
U_{sg} equivalent heat transfer coefficient used to linearize the Stefan–Boltzman equation for IR transfer between the absorber surface and ground (W m^{-2})
U_{ss} equivalent heat transfer coefficient used to linearize the Stephan–Boltzman equation for IR transfer between the absorber surface and sky (W m^{-2})
U_w equivalent heat transfer coefficient for the wind losses on the absorber surface (W m^{-2})
v_i air velocity in "pipe" at position i (m s^{-1})
v_0 face velocity (m s^{-1})

Greek letters

α absorptance of collector surface
δ absorber porosity (hole area/collector area)
ΔP change in pressure (Pa)
$\Delta P_{absorber}$ pressure drop across the absorber (Pa)
$\Delta P_{acceleration}$ acceleration pressure drop inside plenum (Pa)
$\Delta P_{buoyancy}$ buoyancy pressure drop inside plenum (Pa)
$\Delta P_{friction}$ frictional pressure drop inside plenum (Pa)
$\Delta P_{manifold}$ pressure drop across entrance to header or exit (Pa)
ϵ absorber emissivity
ϵ_{hx} absorber heat exchange effectiveness
ρ density of air (kg m^{-3})
$\rho_{ambient}$ density of ambient air (kg m^{-3})
ρ_{ypipe} density of air in y-directional pipe (kg m^{-3})
σ Stefan–Boltzmann constant (5.670×10^{-8} W m^{-2} K^{-4})
υ kinematic viscosity (m^2 s^{-1})

REFERENCES

Acrivos A., Babcock B. D. and Pigford R. L. (1959) Flow distributions in manifolds. *Chem. Engng Sci.* **10,** 112–124.

ASHRAE (1993) *ASHRAE Handbook 1993 Fundamentals.* American Society of Heating, Refrigeration and Air-Conditioning Engineers Inc., Atlanta.

Bajura R. A. and Jones E. H., Jr. (1976) Flow distribution manifolds. *ASME J. Fluids Engng.* **December,** 654–665.

Dymond C. S. (1994) A model of the air flow and temperature distribution of an unglazed transpired solar collector. Master's Thesis, University of Colorado, Boulder, Colorado, U.S.A.

Enermodal Engineering Limited (1994) Performance of the Perforated-Plate/Canopy Solarwall at GM Canada, June.

Gunnewiek L. H. (1994) An investigation of the flow distribution through unglazed transpired-plate solar air heaters. Master's Thesis, University of Waterloo, Waterloo, Canada.

Hollick J. (1995) Conserval Engineering Inc., Downsview, Ontario, Canada, personal communication.

Jeppson R. W. (1976) *Analysis of Flow in Pipe Networks.* Ann Arbor Science Publishers, Ann Arbor, Michigan, U.S.A.

Kutscher C. F. (1994) Heat exchange effectiveness and pressure drop for air flow through perforated plates with and without crosswind. *ASME J. Heat Transfer* **116,**

Kutscher C. F. (1992) An investigation of heat transfer for air flow through low-porosity perforated plates. Ph.D. Dissertation, University of Colorado, Boulder, Colorado, U.S.A.

Kutscher C. F., Christensen C. B. and Barker G. M. (1993) Unglazed transpired solar collectors: heat loss theory. *ASME J. Solar Energy Engng.* **August.**

Pigford R. L., Ashraf M. and Miron Y. D. (1983) Flow distribution in piping manifolds. *Ind. Engng Chem. Fundam.* **22,** 463–471.

Schulz H. (1988) Das Solarzelt (The Solar Tent). Report published by Lantechnik Weihenstephan der TU, Munich, Germany.

Shen P. I. (1992) The effect of friction on flow distribution in dividing and combining flow manifolds. *ASME J. Fluids Engng.* **114,** 121–123.